First-principles study of the formation and electronic structure of a conductive filament in ZnO-based resistive random access memory*

Zhao Jing(赵 晶)[a)b)], Dong Jing-Yu(董静雨)[a)], Ren Shu-Xia(任书霞)[a)c)], Zhang Li-Yong(张礼勇)[a)], Zhao Xu(赵 旭)[a)], and Chen Wei(陈 伟)[a)†]

[a)] *Key Laboratory of Advanced Films of Hebei Province, College of Physics Science & Information Engineering, Hebei Normal University, Shijiazhuang* 050024, *China*

[b)] *Department of Physics and Electrical Engineering, Handan College, Handan* 056005, *China*

[c)] *School of Material Science and Engineering, Shijiazhuang TieDao University, Shijiazhuang* 050043, *China*

(Received 30 July 2014; revised manuscript received 30 August 2014; published online 10 October 2014)

Oxygen vacancy plays a crucial role in resistive switching. To date, a quantitative study about the distribution of the oxygen vacancies and its effect on the resistive switching has not yet been reported. In this study, we report our first-principles calculations in ZnO-based resistive switching memory grown on a Pt substrate. We show that the oxygen vacancies prefer to be located in the ZnO (0001) plane, i.e. in the direction parallel to the film surface in the preparation process. These oxygen vacancies drift easily in the film when a voltage is applied in the SET process and prefer to form a line defect perpendicular to the film surface. An isolated oxygen vacancy makes little contribution to the conductivity of ZnO, whereas the ordering of oxygen vacancies in the direction perpendicular to the film surface leads to a dramatic enhancement of the conductivity and thus forms conductive filaments. The semiconducting characteristics of the conductive filaments are confirmed experimentally.

Keywords: first-principles calculations, resistive switching, conductive filament, oxygen-vacancy ordering

PACS: 73.22.–f, 73.61.–r, 71.55.–i **DOI:** 10.1088/1674-1056/23/12/127301

1. Introduction

The reversible resistive switching (RS) effect in transition metal–oxide thin film has attracted considerable attention because of its potential for next-generation nonvolatile applications such as resistive random access memories.[1–4] Understanding the switching mechanisms is thus a major challenge in achieving better nonvolatile memory performance. At present, several models[5–9] have been proposed to understand RS behavior. Among them, the role of defects, in particular oxygen vacancies, has become a topic of interest. It has been generally accepted that formation and rupture of conductive filaments (CFs) based on oxygen vacancies is responsible for RS between the high resistance state and low resistance state (LRS).[10] However, as far as we know, a quantitative study of the formation and the electronic structure of the CFs has not yet been reported.

Oxygen vacancies are native defects in ZnO films and are inevitable in the preparation process. The distribution of the oxygen vacancies may, however, change during RS due to the migration of oxygen ions under action of an applied electric field, and extensive experimental studies have shown that oxygen vacancies easily migrate in oxide thin films.[10] The electronic property of ZnO has been widely studied using density functional theory (DFT),[11,12] however, the arrangement of oxygen vacancies and its effect on resistive switching in ZnO film has not been reported. How the oxygen vacancies distribute when the films are first prepared, how they redistribute when a voltage is applied during RS, and how the redistribution of oxygen vacancies affects the resistance of the film are questions that remain to be further studied. In this work, we perform first-principles calculations for ZnO thin films with oxygen vacancy defects. The formation and the electronic structure of the CFs is studied systematically.

2. Method and computation details

Our calculations were performed with the CASTEP code,[13] which is based on DFT and the Vanderbilt ultrasoft pseudopotential.[14] The electron-exchange correlation function is treated using the generalized gradient approximation (GGA)[15] with the Perdew–Wang91[16] approach. To give a proper description of the strong correlation effects, GGA + U[17] methods were used. The values of the on-site Coulomb parameter U for the 3d states of Zn and the 2p states of O were taken to be 10.5 eV and 7 eV,[18] respectively. Calculations were performed on a $3\times3\times2$ ZnO supercell with 72 atoms. In order to ensure good convergence of the geometry optimization, the cut-off energy was chosen as 340 eV in all calculations. In order to ensure sufficient accuracy for the self-consistent Brillouin zone integration, a $3\times3\times1$ Monkhorst–Pack k-point mesh was used.

*Project supported by the Natural Science Foundation of Hebei Province, China (Grant Nos. A2013205149 and E2013210133) and the Hebei Provincial Education Department, China (Grant Nos. ZH2012067 and 2011170).

†Corresponding author. E-mail: chen07308@mail.hebtu.edu.cn

© 2014 Chinese Physical Society and IOP Publishing Ltd

3. Results and discussion

To investigate the most stable configuration of the oxygen vacancies, the interaction energy ($E_{\rm int}$) between oxygen vacancies is calculated from the following expression:[19]

$$E_{\rm int} = E\,(n{\rm V_o}) + E\,({\rm ZnO}) - E\,[(n-1)\,{\rm V_o}] - E\,(1{\rm V_o})\,, \quad (1)$$

where E(ZnO) is the total energy of the supercell with no defects, $E\,(n{\rm V_o})$ is the total energy of the supercell with the vacancies whose number is indicated in parenthesis, and n is the number of oxygen vacancies. Figure 1 shows schematically the configuration (a), side (b), and top (c) view of wurtzite ZnO. The oxygen vacancies located at positions a–j are denoted as ${\rm V}_a \sim {\rm V}_j$.

The interaction energies of oxygen vacancies ${\rm V}_b \sim {\rm V}_h$ with vacancy ${\rm V}_a$ are shown in Fig. 1(d). During the calculations, the first oxygen vacancy ${\rm V}_a$ is fixed and the second oxygen vacancy is located at one of the positions labeled ${\rm V}_b \sim {\rm V}_h$ as shown in Fig. 1(a). According to our calculation, when the second oxygen vacancy is in the (0001) plane (positions ${\rm V}_b$, ${\rm V}_c$ or ${\rm V}_d$), the interaction energy is at its lowest. This result is in agreement with that in [20], and implies that the oxygen vacancies prefer to be located in the ZnO (0001) plane in the deposition process. For the RS studies, ZnO films are usually grown using pulsed laser deposition and tend to grow with their c-axis perpendicular to the commonly used Pt substrate surface.[3] This means that the oxygen vacancies prefer to be located in the direction parallel to the film surface in the preparation process.

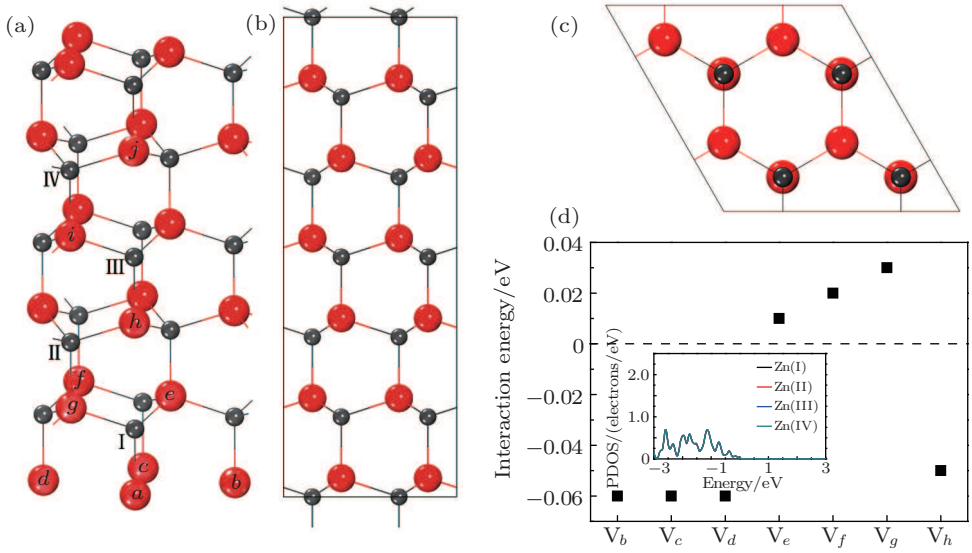


Fig. 1. (color online) Schematic configuration (a), side (b), and top (c) view of wurtzite ZnO. The large balls represent the oxygen atoms and the small balls represent the Zn atoms. The positions of the oxygen atoms are labeled as a–j. The positions of Zn atoms near the oxygen vacancies are labeled I, II, III, and IV. (d) The interaction energy between the first oxygen vacancy (${\rm V}_a$) and the second defect at one of the positions ${\rm V}_b \sim {\rm V}_h$. The inset shows the partial atomic density of states (PDOS) of Zn atoms of $Zn_{36}O_{36}$. The PDOS for all four Zn atoms are indistinguishable.

Note that the interaction energy of ${\rm V}_h$ is only 0.01 eV greater than those of ${\rm V}_b$, ${\rm V}_c$, and ${\rm V}_d$, which implies that the oxygen vacancies at ${\rm V}_b$, ${\rm V}_c$, and ${\rm V}_d$ can easily move to the position of ${\rm V}_h$ if an electric field perpendicular to the film surface is applied in the SET process. The movement of oxygen vacancies is a common phenomenon in various oxide materials. Jeong *et al.*[21] reported the direct observation of oxygen vacancy drift in TiO_2 under action of an applied voltage. Since the line connecting ${\rm V}_a$ and ${\rm V}_h$ is perpendicular to the film surface, following such a migration, the oxygen vacancies would lie in the direction perpendicular rather than parallel to the film surface. It is generally believed that the oxygen vacancies in the as-grown films move toward the bottom electrode when a positive voltage is applied, and form CFs between the bottom and top electrodes.[10] This RS mechanism is in agreement with our calculations described above.

In order to determine the position of the third oxygen vacancy, we compare the interaction energies of ${\rm V}_g$ and ${\rm V}_j$ which are the nearest neighbors of the first two oxygen vacancies, ${\rm V}_a$ and ${\rm V}_h$, as shown in Fig. 1(a). The results show that the value of the interaction energy in the oxygen vacancy structure ${\rm V}_a$, ${\rm V}_h$, ${\rm V}_g$ (-2.257 eV) is smaller than that in the other structure ${\rm V}_a$, ${\rm V}_h$, ${\rm V}_j$ (-2.059 eV). Consequently, we take ${\rm V}_g$ as the third oxygen vacancy. Similarly, ${\rm V}_i$ and ${\rm V}_j$ are tested as the fourth oxygen vacancy. The interaction energy in the oxygen vacancy structure of ${\rm V}_a$, ${\rm V}_h$, ${\rm V}_g$, ${\rm V}_i$ (-2.207 eV) is found to be smaller than in the structure of ${\rm V}_a$, ${\rm V}_h$, ${\rm V}_g$, ${\rm V}_j$ (-2.015 eV), so we take ${\rm V}_i$ as the fourth oxygen vacancy. This

kind of oxygen vacancy ordering in $SrTiO_3$ has been observed directly by Jia *et al.*[22]

The energy band structures of $Zn_{36}O_{36}$ (perfect ZnO), $Zn_{36}O_{35}$ (one oxygen vacancy V_a), $Zn_{36}O_{34}$ (two oxygen vacancies V_a and V_h), $Zn_{36}O_{33}$ (three oxygen vacancies V_a, V_h, and V_g), and $Zn_{36}O_{32}$ (four oxygen vacancies V_a, V_h, V_g, and V_i), calculated using the GGA + U are shown in Fig. 2 where the Fermi level has been taken to be at zero energy. The calculated band-gap width for $Zn_{36}O_{36}$ is $\sim$ 3.42 eV as shown in Fig. 2(a), which is close to the experimental value of 3.43 eV.[23]

For $Zn_{36}O_{35}$ with a single oxygen vacancy, V_a, the defect state is located about 1.112 eV above the valence band maximum as shown in Fig. 2(b). This result indicates that the defect state of an isolated oxygen vacancy is too deep to elevate electrons to the conduction band at room temperature, thus making little contribution to the conductivity of the system. These characteristics are consistent with previous calculations presented by Oba *et al.*[24] However, with additional oxygen vacancies, the defect bands are considerably more spread out and the Fermi level turns closer to the conduction band minimum as shown in Figs. 2(c)–2(e). This means that the energy band-gap of the material decreases dramatically with the further introduction of the oxygen vacancies.

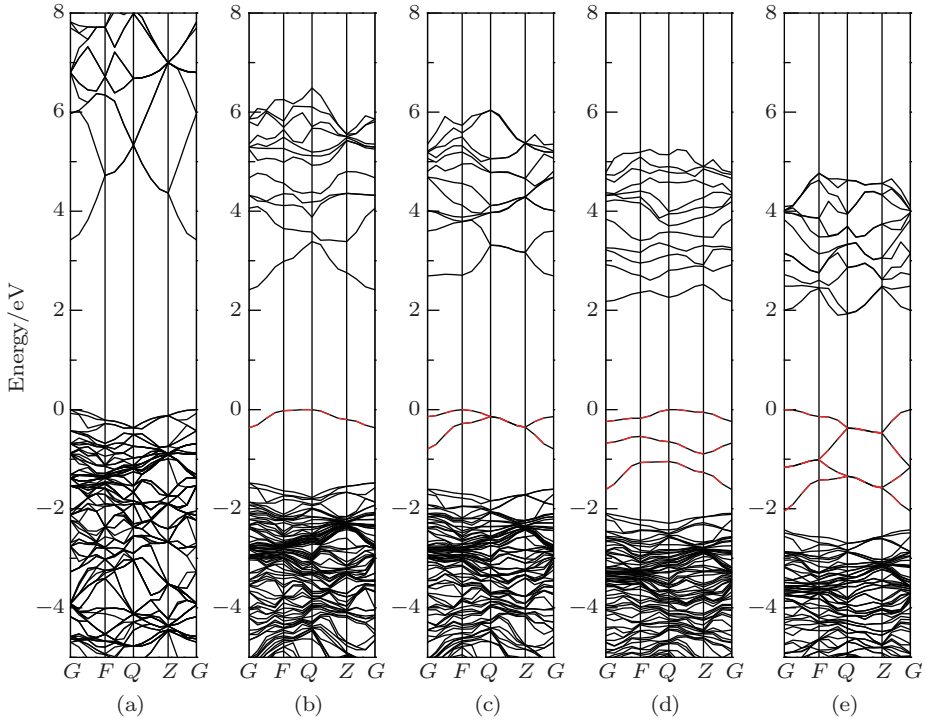


Fig. 2. (color online) Energy band structures of $Zn_{36}O_{36}$ (a), $Zn_{36}O_{35}$ (one oxygen vacancy V_a) (b), $Zn_{36}O_{34}$ (two oxygen vacancies V_a and V_h) (c), $Zn_{36}O_{33}$ (three oxygen vacancies V_a, V_h, and V_g) (d), and $Zn_{36}O_{32}$ (four oxygen vacancies V_a, V_h, V_g, and V_i) (e). The dashed curves represent the defect states.

Figure 3 shows the PDOS of neighboring Zn atoms surrounding the oxygen vacancies (the locations of the Zn atoms are shown in Fig. 1(a) as I–IV) of $Zn_{36}O_{35}$, $Zn_{36}O_{34}$, $Zn_{36}O_{33}$, and $Zn_{36}O_{32}$. The PDOS of the same Zn atoms in $Zn_{36}O_{36}$ is shown in the inset of Fig. 1(d). It can be seen from Fig. 3(a) that the defect state is observed only for the nearest neighbor Zn atoms, I and IV, after the introduction of the first oxygen vacancy V_a, indicating that two electrons occupying the oxygen 2p orbit are highly localized on the Zn atoms I and IV. There is almost no defect state formed in Zn atoms II and III since these atoms are relatively far from the oxygen vacancy V_a. Compared with the scenario of single oxygen vacancy V_a, the introduction of the second vacancy V_h affects the defect states of the Zn atoms I–IV, especially Zn atoms II, III, as shown in Fig. 3(b). This is due to the short distance between Zn atoms II, III, and vacancy V_h. With the introduction of the third oxygen vacancy V_g, the defect states of Zn atoms I–IV spread out considerably, especially in Zn atoms I, II, and IV as shown in Fig. 3(c), showing that the vacancy cluster V_a, V_h, and V_g significantly affects the redistribution of electrons. The result is that a larger proportion of the electrons are localized around Zn atoms I, II, and IV. With the introduction of the fourth oxygen vacancy V_i, the defect states of Zn atoms I–IV are further spread out and defect levels are distributed over a large range in the forbidden band as shown in Fig. 3(d), implying that the electrons are more uniformly localized around the Zn atoms I–IV. As a consequence, the conductivity in this ordered oxygen vacancy channel is improved greatly and thus forms the conductive filament.

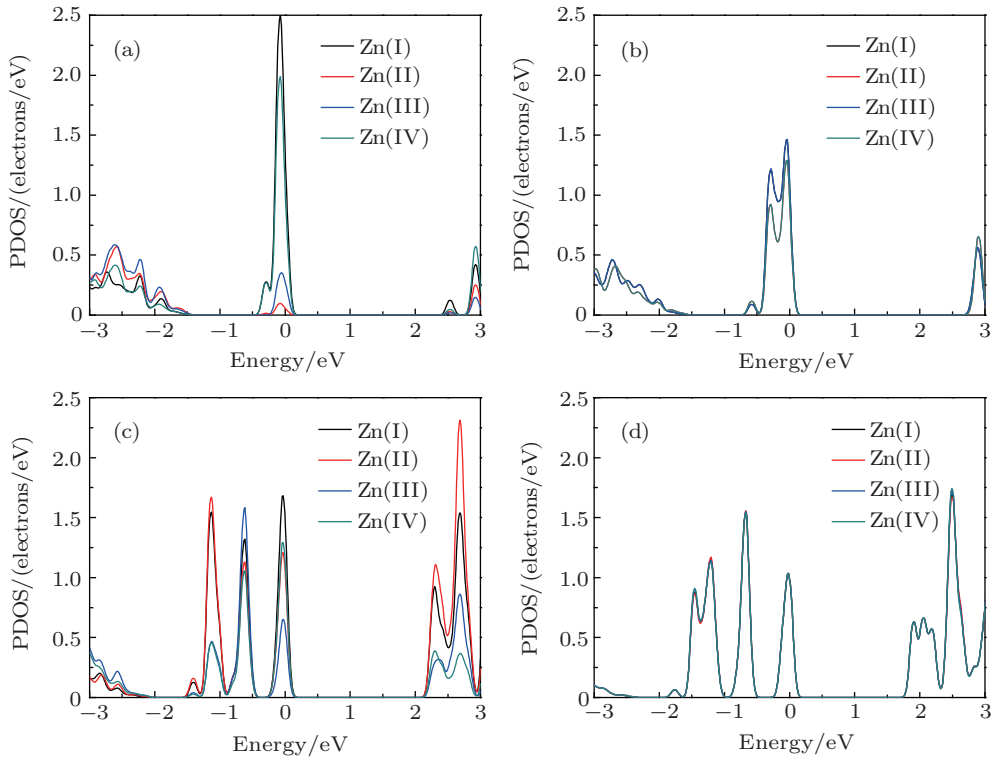


Fig. 3. (color online) The PDOSs of neighboring Zn atoms I–IV surrounding the oxygen vacancies in $Zn_{36}O_{35}$ (a), $Zn_{36}O_{34}$ (b), $Zn_{36}O_{33}$ (c), and $Zn_{36}O_{32}$ (d). The PDOSs of Zn atoms I and III are overlapped and the PDOSs of Zn atoms II and IV are overlapped in part (b). There is almost no color for (d) since the PDOS curves overlap.

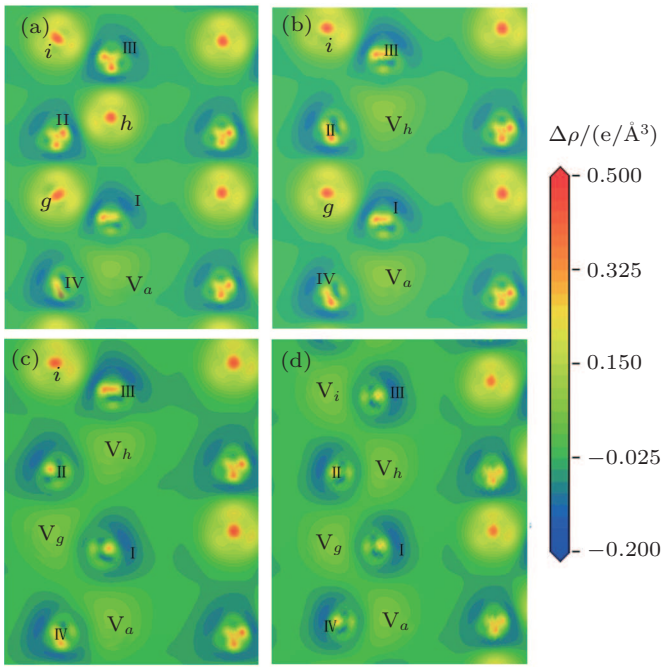


Fig. 4. (color online) Charge density difference contour plots for $Zn_{36}O_{35}$ (a), $Zn_{36}O_{34}$ (b), $Zn_{36}O_{33}$ (c), and $Zn_{36}O_{32}$ (d) in the $(10\bar{1}0)$ plane. In all four parts, the scale of the charge density difference runs from -0.2 e/Å^3 to $+0.5$ e/Å^3.

In order to demonstrate the electron transport directly, we also plot the charge density difference contours for $Zn_{36}O_{35}$, $Zn_{36}O_{34}$, $Zn_{36}O_{33}$, and $Zn_{36}O_{32}$ in the $(10\bar{1}0)$ plane in Fig. 4. With the introduction of V_a, the charge density of Zn atoms I and IV near V_a increases significantly as shown in Fig. 4(a), indicating that a portion of the electrons that previously hybridized with the O 2p orbit transfer to Zn atoms I and IV. Thus Zn atoms I and IV are reduced and become more metallic. The charge densities of Zn atoms II and III are less affected by V_a. By introducing the second vacancy V_h, the charge densities of Zn atoms II and III increase significantly as shown in Fig. 4(b), implying that Zn atoms II and III are reduced by the vacancy V_h. When we introduce the oxygen vacancies V_g, the charge densities of the Zn atoms I–IV are further increased as shown in Fig. 4(c). This result reveals that a greater portion of electrons transfer to the Zn atoms I–IV and reduce them to a lower chemical state. After the introduction of the fourth oxygen vacancy V_i, the charge densities of all four Zn atoms I–IV are increased and become identical as shown in Fig. 4(d), implying that the four Zn atoms I–IV are all reduced to the same chemical state by the vacancies V_i. As a consequence, a structure with ordered oxygen vacancies tends to make neighboring Zn atoms more metallic, thus the electrons may be transported through this oxygen-vacancy ordered structure more easily. This result is consistent with the calculated PDOS as shown in Fig. 3.

From the above analyses, we can see that with the increase in the number of oxygen vacancies in the direction perpendicular to the film surface, each neighboring Zn^{2+} cation tends to be reduced to the metallic state by redistributing the electrons. These line defects composed of ordered oxygen va-

cancies create a conductive path in the insulating ZnO matrix, thus causing the system to enter the low resistance state. Figure 5(a) shows a schematic structure of the conductive filament in the insulating ZnO matrix. It seems logical that when a reverse electric field is applied to the system, the oxygen vacancies will be drawn back toward the top electrode and the configuration of oxygen vacancies will be destroyed. Thus the system will RESET to the high resistance state.

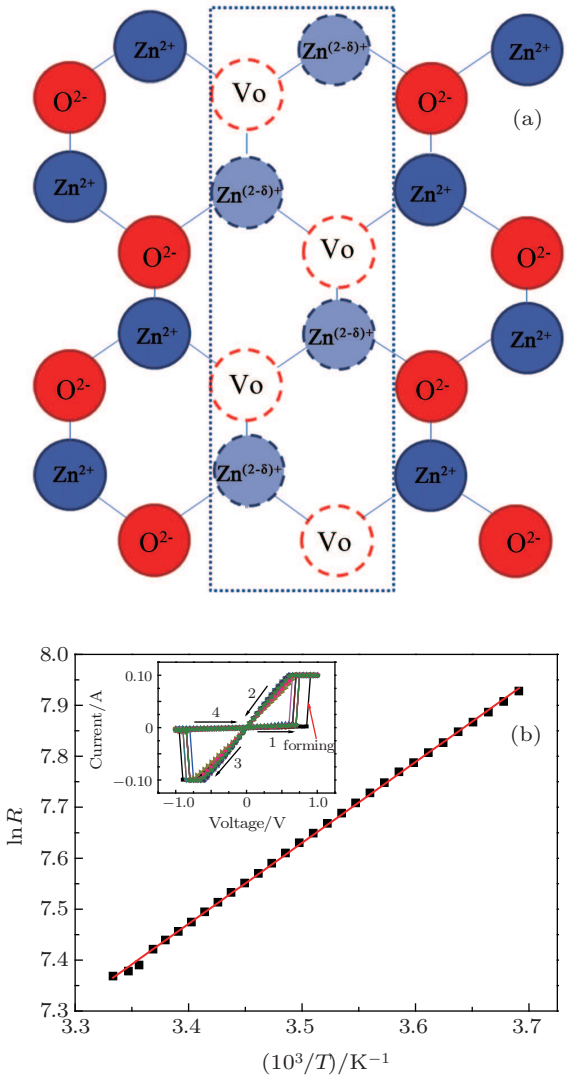


Fig. 5. (color online) (a) Schematic structure of the conductive filament in the insulating ZnO matrix. (b) Plot of resistance versus reciprocal of the temperature for Ti/ZnO/Pt ReRAM in a low resistance state. The inset shows the *I*–*V* characteristics for this device.

The conductivity in the region with ordered oxygen vacancies, namely in the CFs, is improved greatly. However, the conduction is still semiconductive rather than metallic in characteristic. In order to check the semiconducting characteristics of the CFs, it is necessary to measure the temperature dependence of the resistance in the LRS. To test this idea, a Ti/ZnO/Pt sandwich structure is prepared as in our previous work.[3] The inset of Fig. 5(b) shows the *I*–*V* characteristics of the ZnO film which displays a typical bipolar resistive switching behavior. Figure 5(b) shows the measured resistance as a function of the inverse of the temperature of the ZnO film in the LRS. It may be seen that the resistance exhibits an exponential decrease with a temperature increase and follows a thermally activated Arrhenius law:

$$R = R_0 \exp\left(E_a/kT\right), \tag{2}$$

where R_0 is the extrapolated resistance at infinite T, k is the Boltzmann constant, and E_a is the activation energy of the conduction.[25] This temperature dependence of resistance confirms the semiconductor-like behavior of the CFs and is consistent with previously reported behavior.[25,26] The calculated value of E_a is about 0.14 eV, indicating that the energy band-gap is reduced to about 0.28 eV due to a large number of oxygen vacancies existing in the conductive filament.[25]

4. Conclusions

In this paper, our calculations show that the oxygen vacancies prefer to be located in the ZnO (0001) plane, i.e. in the direction parallel to the film surface in the preparation process. These oxygen vacancies drift easily to form a line defect in the direction perpendicular to the film surface when a voltage is applied in the SET process. With the number of ordered oxygen vacancies increasing in the direction perpendicular to the film surface, the defect bands are considerably dispersed and the Fermi level moves closer to the conduction band minimum. Oxygen vacancy ordering causes chemical reduction of their neighboring Zn ions by redistributing the electrons, thus the conductivity is greatly improved along the line defects. This mechanism is also applicable to other binary metal–oxide system such as TiO_2 and HfO_2.

Acknowledgment

The authors are grateful to Dr Tian Zhi-Xue for helpful discussion and Prof Norm Davison for critical reading of the manuscript.

References

[1] Sawa A 2008 *Mater. Today* **11** 28
[2] Hong D S, Chen Y S, Li Y, Yang H W, Wei L L, Shen B G and Sun J R 2014 *Sci. Rep.* **4** 04058
[3] Ren S X, Sun G W, Zhao J, Dong J Y, Wei Y, Ma Z C, Zhao X and Chen W 2014 *Appl. Phys. Lett.* **104** 232406
[4] Zhao J W, Liu F J, Huang H Q, Hu Z F and Zhang X Q 2012 *Chin. Phys. B* **21** 065201
[5] Chen A, Haddad S, Wu Y C, Lan Z, Fang T N and Kaza S 2007 *Appl. Phys. Lett.* **91** 123517
[6] Kim D C, Seo S, Ahn S E, Suh D S, Lee M J, Park B H, Yoo I K, Baek I G, Kim H J, Yim E K, Lee J E, Park S O, Kim H S, Chung U I, Moon J T and Ryu B I 2006 *Appl. Phys. Lett.* **88** 202102
[7] Fujii T, Kawasaki M, Sawa A, Akoh H, Kawazoe Y and Tokura Y 2005 *Appl. Phys. Lett.* **86** 012107
[8] Guo X, Schindler C, Menzel S and Waser R 2007 *Appl. Phys. Lett.* **91** 133513
[9] Waser R, Dittmann R, Staikov G and Szot K 2009 *Adv. Mater.* **21** 2632
[10] Xu N, Liu L, Sun X, Liu X, Han D, Wang Y, Han R, Kang J and Yu B 2008 *Appl. Phys. Lett.* **92** 232112

[11] Zhang H, Wu D, Tang Q, Liu L and Zhou Z 2013 *J. Mater. Chem. A* **1** 2231

[12] Xu P, Tang Q and Zhou Z 2013 *Nanotechnology* **24** 305401

[13] Segall M D, Philip J D L, Probert M J, Pickard C J, Hasnip P J, Clark S J and Payne M C 2002 *J. Phys.: Condens. Matter* **14** 2717

[14] Vanderbilt D 1990 *Phys. Rev. B* **41** 7892

[15] Perdew J P, Burke K and Ernzerhof M 1996 *Phys. Rev. Lett.* **77** 3865

[16] Perdew J P, Chevary J A, Vosko S H, Jackson K A, Pederson M R, Singh D J and Fiolhais C 1992 *Phys. Rev. B* **46** 6671

[17] Anisimov V I, Zaanen J and Andersen O K 1991 *Phys. Rev. B* **44** 943

[18] Sheetz R M, Ponomareva I, Richter E, Andriotis A N and Menon M 2009 *Phys. Rev. B* **80** 195314

[19] Park S, Ahn H S, Lee C K, Kim H, Jin H, Lee H S, Seo S, Yu J and Han S 2008 *Phys. Rev. B* **77** 134103

[20] Wang Q, Sun Q, Jena P and Kawazoe Y 2009 *Phys. Rev. B* **79** 115407

[21] Jeong H Y, Lee J Y and Choi S Y 2010 *Appl. Phys. Lett.* **97** 042109

[22] Jia C L, Lentzen M and Urban K 2003 *Science* **299** 870

[23] Reynolds D C, Look D C, Jogai B, Litton C W, Cantwell G and Harsch W C 1999 *Phys. Rev. B* **60** 2340

[24] Oba F, Togo A, Tanaka I, Paier J and Kresse G 2008 *Phys. Rev. B* **77** 245202

[25] De Stefano F, Houssa M, Kittl J A, Jurczak M, Afanasév V V and Stesmans A 2012 *Appl. Phys. Lett.* **100** 142102

[26] Chen G, Song C, Chen C, Gao S, Zeng F and Pan F 2012 *Adv. Mater.* **24** 3515